*Article*

# Testing Screening Mechanisms with Mass Profiles of Galaxy Clusters

**Lorenzo Pizzuti** [ID]

Osservatorio Astronomico della Regione Autonoma Valle d'Aosta, Loc. Lignan 39, 11020 Nus, Italy; pizzuti@oavda.it

**Abstract:** We present MG-MAMPOSSt, a license-free code to constrain modified gravity models by reconstructing the mass profile of galaxy clusters with the kinematics of the cluster's member galaxies. We describe the main features of the code and we show the capability of the method when the kinematic information is combined with lensing data. We discuss recent results and forecasts on two classes of models currently implemented in the code, characterized by different screening mechanisms, namely, chameleon and Vainshtein screening. We further explore the impact of possible systematics in view of application to the data from upcoming surveys.

**Keywords:** comsology; galaxy clusters; dark energy; modified gravity

## 1. Introduction

Scalar–tensor theories of gravity represent one of the most general classes of modified gravity (MG) models viable at cosmological scales, characterized by a quite large number of interesting features (see, e.g., [1]). This family of theories includes several subclasses, such as the Horndeski (e.g., [2]) and the more general Degenerate Higher-Order Scalar–Tensor (DHOST hereafter) theories (e.g., [3,4]).

A new dynamical scalar field propagates an additional fifth force which enhances gravity locally on sufficiently large scales, producing possible detectable imprints on the formation and evolution of cosmological structures. In order to match observational constraints on small scales and dense environments, the fifth force should be further suppressed through a so-called screening mechanism, which relies on the non-linear interaction of the scalar field (e.g., [5]).

In this framework, galaxy clusters constitute a powerful tool to investigate modification of gravity at large scales (see [6] for a recent review); in particular, with the combination of the cluster's mass profiles derived with lensing and internal kinematic analyses of the hot intra-cluster gas (e.g., [7–9]) and of cluster's member galaxies (e.g., [10,11]), it is possible to constrain departures from General Relativity (GR) in a complementary way with respect to other cosmological and astrophysical observations.

To this end, we developed MG-MAMPOSSt, a FORTRAN code which determines cluster mass profiles in modified gravity from the kinematics of cluster members; the program is based upon the MAMPOSSt method of [12]. While the latter assumes that the gravitational interaction is described by GR, MG-MAMPOSSt explores two popular and quite general classes of MG models, characterized by distinct screening mechanisms: chameleon screening (CS) and Vainshtein screening (VS).

The code further implements a lensing simulation to investigate the capability of a joint lensing and kinematic analysis to constrain the free parameters of the models. The code has been recently made publicly available[1].

Here we apply the method over a mock catalogue of dark matter haloes to forecast the constraints on the parameters in the two classes of models cited above, obtainable by current and future kinematic and lensing measurements of galaxy cluster mass profiles. This paper summarizes the results presented at the ALTECOSMOFUN'21 conference and

is based upon the works of Pizzuti et al. published in 2020, 2021 and 2022. In Section 2, we provide a brief overview of the MG models implemented, in Section 3 the main features of MG-MAMPOSSᴛ are presented while in Section 4 we show our results and preliminary outcomes from the application of MG-MAMPOSSᴛ over real data. Finally, a summary and a discussion about systematics are provided in Section 5.

## 2. Theoretical Background

In scalar–tensor theories, the screening of the fifth force operates in different ways depending on the non-linear interactions of the field.

Models which implement the chameleon mechanism—typically conformally coupled models such as $f(\mathcal{R})$ gravity, [14]—rely on the potential of the field to make the mass of the scalar very large at small scales, such that the fifth force does not propagate. In CS, the usual Newtonian potential is modified by an additional term which depends on the gradients of the scalar field $\phi$ (see e.g., [15,16]),

$$\frac{d\Phi}{dr} = \frac{GM(r)}{r^2} + \frac{\mathcal{Q}}{M_{\mathrm{P}}}\frac{d\phi}{dr}. \tag{1}$$

where $M(r)$ is the total mass enclosed within a sphere of radius $r$, $M_{\mathrm{P}} = (8\pi G)^{-1/2}$ is the reduced Planck mass, $G$ is the Newton's constant and $\mathcal{Q}$ is a dimensionless coupling constant[2] which can assume different values depending on the specific theory. The case of $f(\mathcal{R})$ gravity, where the Einstein–Hilbert action is modified by adding a general non-linear function of the Ricci curvature scalar $R$, can be shown to be conformally equivalent to a subclass of chameleon models where $\mathcal{Q} = 1/\sqrt{6}$ (see e.g., [17]). In the above Equation (1) spherical symmetry has been assumed.

The explicit expression of the field profile depends on the matter density distribution $\rho(r)$. Here we use the Navarro–Frenk–White (NFW) profile of [18] to model the matter density in MG frameworks, which has been shown to provide an overall good description of the total mass profile of cluster-size halos in equilibrium configuration from cosmological simulations and observational data in GR (e.g., [19]) and in MG (e.g., [20]). Nevertheless, the MG-MAMPOSSᴛ method can be easily extended to other mass models in non-standard frameworks. The NFW model is fully specified by the scale radius $r_{\mathrm{s}}$ at which the logarithmic derivative of the profile is equal to $-2$ and the "virial" radius $r_{200}$ encloses an overdensity 200 times the critical density of the universe.

Given the NFW model for $\rho(r)$, we solve Equation (1) to obtain the field profile inside (where field gradients are negligilble) and outside the source (where the potential is subdominant) by assuming the same analytical approximation of e.g., [7],

$$\phi(x) = \begin{cases} \sim 0 & r < S \\ -\dfrac{\mathcal{Q}\rho_{\mathrm{s}} r_{\mathrm{s}}^2}{M_{\mathrm{P}}}\dfrac{\ln(1+x)}{x} - \dfrac{C}{x} + \phi_\infty & r > S. \end{cases} \tag{2}$$

In the above equation $\rho_{\mathrm{s}}(r_{\mathrm{s}}, r_{200})$ is the characteristic density of the NFW model, $\phi_\infty$ is the background value of the field, $C$ is an integration constant and $x = r/r_{\mathrm{s}}$. The solutions match at the *screening radius S*. Requiring the continuity of the function and of its first derivative at the matching point, $C$ and $S$ are fully specified in terms of $(r_{200}, r_{\mathrm{s}}, \mathcal{Q}, \phi_\infty)$. In particular, the screening radius depends on $r_{200}^3$. Thus, haloes with different masses exhibit a less/more efficient chameleon mechanism.

In CS, due to the conformal structure of the models, photon propagation is not affected by the fifth force. This can be seen by the definition of the lensing potential $\Phi_{\mathrm{lens}}$ which, at linear order, is given by the sum of the potential $\Phi$ and the relativistic potential $\Psi$. The contribution of the fifth force appears with opposite sign in the two terms and cancels out (see e.g., [16]). This means that lensing observations are sensitive only to the standard Newtonian potential.

In Vainsthein screening, which is a typical feature of DHOST theories, the suppression of the fifth force is achieved by working on higher-order derivatives of the field. In this case the mechanism to recover GR can be partly broken inside a massive object, giving rise to a fifth force which depends on the gradients of the matter distribution (see e.g., [21]). Assuming spherical symmetry and an NFW model for the matter density distribution, the Poisson equation associated with the Newtonian potential $\Phi$ (which governs the dynamics of galaxies and gas in clusters) is modified according to (e.g., [9]):

$$\frac{d\Phi}{dr} \equiv \frac{GM_{\rm dyn}}{r^2} = \frac{G}{r^2}\left[M_{\rm NFW}(r) + M_{200}\frac{Y_1}{4}\frac{r^2(r_{\rm s}-r)}{(r_{\rm s}+r)^3} \times [\ln(1+c) - c/(1+c)]^{-1}\right], \quad (3)$$

where $M_{\rm NFW}(r)$ is the NFW mass profile, $M_{200}$ is the mass of a sphere of radius $r_{200}$ enclosing an average density 200 times the critical density of the universe and $c = r_{200}/r_s$ is called concentration. Finally, $Y_1$ is a dimensionless parameter describing the fifth force coupling.

In this class of models, photon propagation is explicitly modified. In particular, the relativistic potential $\Psi$ receives a contribution form the fifth force, giving rise to an effective lensing mass (e.g., [22]):

$$M_{\rm lens}(r) = \frac{r^2}{2G}\left[\frac{d\Psi}{dr} + \frac{d\Phi}{dr}\right] = M_{\rm dyn} + M_2, \quad (4)$$

where

$$M_2 = -\frac{5}{4}Y_2\frac{r^2 M_{200}}{[\ln(1+c) - c/(1+c)]}\frac{(r_{\rm s}+r)}{(r_{\rm s}+r)^3}. \quad (5)$$

The coupling $Y_2$ appears only in the relativistic sector, i.e., it can be constrained only by lensing observations. Current constraints for $Y_1$ are of the order of $10^{-2}$ as obtained from stellar probes (e.g., [23,24]), and of $10^{-1}$ at the cosmological level with galaxy clusters (e.g., [25,26]). As for $Y_2$, only cosmological bounds are available ($\mathcal{O}(1)$ from [9] and $\mathcal{O}(0.1)$ from [26], which worked on a generalization of the model presented here).

## 3. The MG-MAMPOSST Method

MG-MAMPOSST is a code aimed at constraining modified gravity models by analysing the kinematics of cluster member galaxies. Derived from the original MAMPOSST method[3] of [12], the program was first presented in a preliminary version in [11], and then extended and updated by [22]. The latest version implements both the CS and VS parametrization of the gravitational potentials described in Section 2, based on the NFW model for the matter density profile.

The input data-set of the MAMPOSST and MG-MAMPOSST procedure is the projected phase space (p.p.s.) of the member galaxies $(R, v_z)$, where $R$ is the projected radius from the cluster center and $v_z$ represents the line-of-sight (l.o.s.) velocity, computed in the rest frame of the cluster. Assuming dynamical relaxation (i.e., galaxies are collisonless tracers of the gravitational potential) and a Gaussian modelling of the three-dimensional velocity distribution, the codes computes orbits of cluster members by solving the (stationary) spherical Jeans' equation to obtain the velocity dispersion profile along the radial direction $\sigma_r^2$ (see e.g., [27]):

$$\sigma_r^2(r) = \frac{1}{\nu(r)}\int_r^\infty \exp\left[2\int_r^s\frac{\beta(t)}{t}dt\right]\nu(s)\frac{d\Phi}{ds}ds, \quad (6)$$

where $\nu(r)$ corresponds to the number density profile of tracers, $\beta \equiv 1 - (\sigma_\theta^2 + \sigma_\phi^2)/2\sigma_r^2$ is the velocity anisotropy profile and $\Phi$ is the total gravitational potential, which carries information about the nature of the gravitational interaction (e.g., Equations (1) and (3)).

Given a parametric expression for the above mentioned quantities, MG-MAMPOSST performs a Maximum Likelihood estimation of the model parameters using data of the p.p.s. In particular, the code computes the probability that a member galaxy found at the

point $(R_i, v_{z,i})$ in the p.p.s. belongs to the orbits distribution described by the model(s). In the most general case, the code can work with six free parameters, namely two mass profile parameters (e.g., $r_{200}$, $r_s$), one parameter for the scaling of the number density profile $r_\nu$[4], one parameter describing the velocity anisotropy profile $\beta$, and two parameters defining the MG model to be constrained ($\mathcal{Q}, \phi_\infty$ for CS and $Y_1, Y_2$ for VS).

The number density $\nu(r)$ can be, in general, excluded from the MG-MAMPOSST fit as it can be measured directly by analysing the projected distribution in the phase space. In the following, we assume an NFW profile to model the galaxy density profile. As for the velocity anisotropy, six possible parametrizations of $\beta(r)$ are currently available in the code (see the technical manual [13]). As a case study, here we adopt the Tiret anisotropy model of [29],

$$\beta_T(r) = \beta_\infty \frac{r}{1 + r_\beta}, \tag{7}$$

where $\beta_\infty$ is the velocity anisotropy for $r \to \infty$ and $r_\beta$ is the characteristic radius of $\beta_T(r)$ (anisotropy radius). In the current version of the code, $r_\beta$ is assumed to be equal to the scale radius of the mass profile $r_s$. Moreover, hereafter we will work with the re-scaled anisotropy parameter $\mathcal{A}_\infty = (1 - \beta_\infty)^{-1/2}$.

The parameter space can be explored either by computing the likelihood over a multi-dimensional grid of values, or by performing a Monte Carlo Markov Chain (MCMC) based on a simple Metropolis–Hastings algorithm with a fixed-step Gaussian random walk. The code takes few hours to produce a complete chain of $\sim 10^5$ points.

Another feature introduced in MG-MAMPOSST is the possibility to simulate additional lensing information to be combined with the likelihood from internal kinematics. This is straightforward in the case of CS where lensing is not affected by the fifth force contribution; the lensing distribution is modeled as a Gaussian $P_{\text{lens}}(r_s, r_{200})$ for the NFW mass profile parameters $r_{200}$, $r_s$. The central values, the standard deviations and the correlation defining the distribution can be customized by the user. In the forecast analysis presented in Section 4, we will assume the lensing Gaussian is centered on the true values of the cluster mass profile's parameters.

The case of VS requires a full lensing simulation, as the lensing mass is explicitly modified in terms of the two fifth-force couplings $Y_1$, $Y_2$. In MG-MAMPOSST, we implemented a simple weak-lensing simulation which generates a mock reduced tangential shear profile assuming a fiducial NFW model in GR. The log-likelihood is given by

$$\ln \mathcal{L}_{\text{lens}}(\boldsymbol{\theta}_l) = -\frac{1}{2} \sum_{i=1}^{N_b} \frac{[\langle g_t(R_i) \rangle - \langle g_{t,\text{vs}}(R_i | \boldsymbol{\theta}_l) \rangle]^2}{\sigma_{l,i}^2}, \tag{8}$$

where $\langle g_t(R_i) \rangle$ is the simulated averaged reduced tangential shear profile at projected position $R_i$, $\langle g_{t,\text{vs}}(R_i)|\theta_l) \rangle$ is the theoretical profile computed in VS for the set of parameters $\boldsymbol{\theta}_l = (r_s, r_{200}, Y_1, Y_2)$.

The number of bins is fixed to $N_b = 10$ (in agreement with current lensing surveys, e.g., [30]) in the projected radial range $[0.12 R_{\text{up}}, 2.9 R_{\text{up}}]$, where $R_{\text{up}}$ is the maximum value of the projected radius a galaxy can have to be considered in the MG-MAMPOSSt fit (see Section 4). The uncertainties are given by the quadratic sum of two contributions:

$$\sigma_{l,i}^2 = \sigma_{e,i}^2 + \sigma_{\text{lss}}^2, \tag{9}$$

where $\sigma_{e,i}^2 = \sigma_g^2 / [\pi(\alpha_{\text{up}}^2 - \alpha_{\text{low}}^2)n_g]$ is the noise due to the intrinsic ellipticity $\sigma_g^2$ of the sources lying within an annulus between the angles $\alpha_{\text{low}}$ and $\alpha_{\text{up}}$, and $\sigma_{\text{lss}}^2$ is the uncertainty due to the projected large-scale structure. The average number of source galaxies per arcmin$^2$ is given by $n_g$. The central values of the NFW parameters from which the shear profile is derived, as well as the lensing uncertainties and $n_g$ can manually set in the input file of MG-MAMPOSST.

## 4. Results

### 4.1. Synthetic Halo Catalogue

The mock catalogue of dark matter haloes used to test MG-MAMPOSST has been produced with the CLUSTERGEN code (e.g., [31]), a generator of spherically symmetric, isolated distributions of particles in dynamical equilibrium, characterized by Gaussian 3D velocity distributions. We assume that all the systematics are under control, i.e., particles in each halo follow an NFW distribution and their velocity is assigned by assuming that $\sigma_r^2$ is given by Equation (6). As for the other velocity dispersion components, $\sigma_\theta^2 \equiv \sigma_\phi^2 = [1 - \beta(r)]\sigma_r^2$. We will comment on the effect of systematics in Section 5. It is important to point out here that a more rigorous way to compute orbits of a spherical system in dynamical equilibrium is to use six-dimensional distribution functions (e.g., [32,33]). A new version of CLUSTERGEN based on this methodology is currently under development.

We considered a total of 20 synthetic massive cluster-size haloes generated in GR[5], as a reasonable number of relaxed galaxy clusters for which high-quality data could be available from upcoming surveys. All haloes are different realizations of the same NFW distribution with $r_{200} = 2.0$ Mpc and $r_s = 0.3$ Mpc. For the case of CS, since the true values of the NFW parameters affect the results, we will further discuss how the constraints change when varying the mass of the synthetic cluster.

For each halo we generated two p.p.s., obtained by considering 600 and 100 particles within the radial range $[0.05 \text{ Mpc}, r_{200}]$, as an optimistic expectation of the number of member galaxies' spectroscopic redshifts available from upcoming surveys, although not unrealistic. The bounds of the radial range are set in spite of real observations, to exclude the cluster core where the Brightest Central Galaxy (BCG) dominates the internal dynamics. As for the upper bound, we adopt the conservative limit of $R_{up} = r_{200}$ to ensure the validity of the Jeans' equation. Finally, as mentioned in Section 3, we consider a Tiret model for the velocity anisotropy profile with $\beta_\infty = 0.5$ (i.e., $\mathcal{A}_\infty = 1.41$).

### 4.2. Vainsthein Screening

We apply the MG-MAMPOSST method to the synthetic p.p.s. with additional simulated lensing information, assuming the VS parametrization for the gravitational potentials, Equations (3) and (4), to constrain the set of parameters $r_{200}$, $r_s$, $\mathcal{A}_\infty$, $Y_1$, $Y_2$. Assuming uniform uninformative priors on each parameter, we perform an MCMC sampling of the joint likelihood:

$$\ln \mathcal{L}_{joint} = \ln \mathcal{L}_{tot}(r_s, r_{200}, \mathcal{A}_\infty, Y_1) + N_h \ln \mathcal{L}_{lens}(\boldsymbol{\theta}_l),$$

where

$$\ln \mathcal{L}_{tot} = \sum_i^{N_h} \left( \ln \mathcal{L}_i^{dyn} \right), \tag{10}$$

is the total MG-MAMPOSST likelihood obtained by combining the information of $N_h$ phase spaces, with $N_h = 1 \ldots 20$.

As for the lensing simulation, we have set $n_g = 30$ arcmin$^{-2}$, as expected for the Wide Survey of the Euclid mission [34], $\sigma_{lss} = 0.005$ and $\sigma_g = 0.3$.

The results of our forecast are summarized in Figure 1 for one p.p.s. with 600 tracers and in columns two to four of Table 1. While for $Y_1$ we cannot obtain competitive bounds with respect to stellar probes, even when increasing the number of haloes in the fit, the relativistic coupling $Y_2$ can be constrained at the level of $\mathcal{O}(0.1)$ already with a few clusters, in agreement with the results of [26] and with a $\sim$2–3 times improvement with respect to the analysis of [9]. In particular, for a single halo we obtain $Y_2 = 0.08_{-0.28}^{+0.32}$ (600 tracers) and $Y_2 = 0.10_{-0.40}^{+0.44}$ (100 tracers).
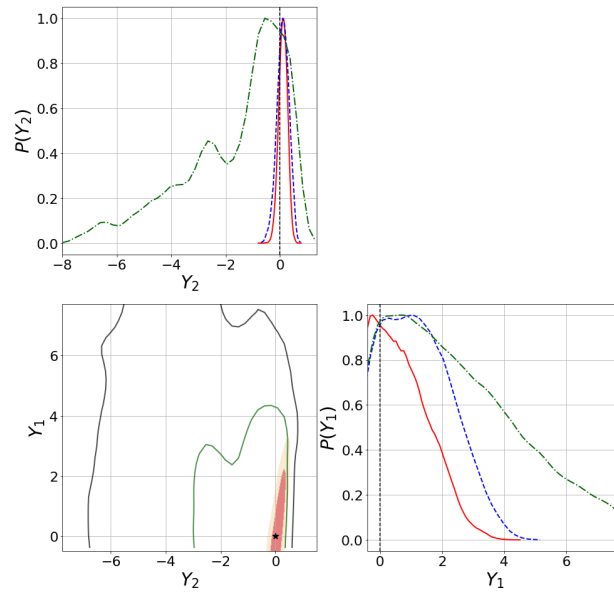
**Figure 1.** Results for the MG-MAMPOSST and lensing forecast in VS for one halo in the sample. (**Bottom-left plot**): confidence regions in the space $(Y_1, Y_2)$. Dark and light red areas and green and black contours represent the $1\sigma$ and $2\sigma$ regions for the internal kinematic and lensing analysis with 600 tracers and for the lensing simulation only, respectively. (**Upper and bottom-right plots**): marginal posteriors of $Y_1$ and $Y_2$. Red lines are for the lensing and kinematics analysis with $N = 600$ tracers, blue dashed curves are for the case with $N = 100$ tracers and green dash-dotted curves show the lensing-only distributions. The GR expectation (i.e., $Y_1 = Y_2 = 0$) is indicated by the black vertical dashed lines. From [22].

**Table 1.** Constraints at 95% C.L obtained for the parameters of the two modified gravity models presented in this work applying the MG-MAMPOSST fit with additional lensing information over the mock catalogue of synthetic halos with $r_{200} = 2.0 \, \text{Mpc}$ and $r_s = 0.3 \, \text{Mpc}$. From column two to column six: Vainshtein screening. Column seven and eight: scalaron field in general chameleon $f(\mathcal{R})$ gravity, related to chameleon field $\phi_\infty$ through Equation (13). For both models we show the results when using $\sim$600 and $\sim$100 cluster members in the MG-MAMPOSST fit.

| | Vainshtein Screening | | | | $f(\mathcal{R})$ Gravity | |
|---|---|---|---|---|---|---|
| | $N = 600$ | | $N = 100$ | | $N = 600$ | $N = 100$ |
| $N_h$ Clusters | $Y_1$ | $Y_2$ | $Y_1$ | $Y_2$ | $\|f_{\mathcal{R}0}\|$ | $\|f_{\mathcal{R}0}\|$ |
| 1 | $\lesssim 2.75$ | $0.08^{+0.32}_{-0.28}$ | $\lesssim 3.56$ | $0.10^{+0.44}_{-0.40}$ | – | – |
| 5 | $\lesssim 1.65$ | $0.06^{+0.20}_{-0.18}$ | $\lesssim 1.87$ | $-0.08^{+0.31}_{-0.20}$ | $\lesssim 3.37 \times 10^{-5}$ | $\lesssim 5.13 \times 10^{-5}$ |
| 10 | $\lesssim 1.24$ | $-0.05^{+0.17}_{-0.13}$ | $\lesssim 1.65$ | $0.01^{+0.24}_{-0.17}$ | $\lesssim 1.12 \times 10^{-5}$ | $\lesssim 3.24 \times 10^{-5}$ |
| 15 | $0.04^{+1.00}_{-0.39}$ | $0.01^{+0.12}_{-0.09}$ | $\lesssim 1.20$ | $-0.01^{+0.19}_{-0.16}$ | $\lesssim 9.51 \times 10^{-6}$ | $\lesssim 2.43 \times 10^{-5}$ |
| 20 | $0.08^{+0.77}_{-0.34}$ | $0.01^{+0.09}_{-0.08}$ | $\lesssim 1.02$ | $0.01^{+0.16}_{-0.14}$ | $\lesssim 7.11 \times 10^{-6}$ | $\lesssim 1.79 \times 10^{-5}$ |

As a preliminary application of MG-MAMPOSST over real data, we further use the high-precision kinematic and lensing information for the massive relaxed cluster MACS J1206.2-0847 (MACS 1206 hereafter) at redshift $z = 0.44$, analysed within the Cluster Lensing and Supernova Survey with Hubble (CLASH, [35]) and CLASH-VLT [36] collaborations, to constrain $Y_1$ and $Y_2$ in VS (see [37] for details). In this case, we have combined the Jeans' analysis of 375 cluster member galaxies in the p.p.s. with the strong plus weak lensing data of [30]. The results of

$$Y_1 < 4.85 \, (\text{stat}) \pm 0.2 (\text{syst}) \quad Y_2 = -0.12^{+0.66}_{-0.67} (\text{stat}) \pm 0.21 \, (\text{syst}), \tag{11}$$

are in very good agreement with the prediction of our forecast analysis. In the above equation, the systematic uncertainties encapsulate the effect of changing the parametrization of the velocity anisotropy profile and the value of the scale radius of the number density profile $r_\nu$ which, as mentioned above, is given by an external fit of the p.p.s.

### 4.3. Chameleon Screening

In this case, the MG parameters defining the model are $\phi_\infty$ and $\mathcal{Q}$. As for VS, we perform an MCMC sampling of the joint kinematic and lensing likelihood. In the Gaussian distribution $P_{\text{lens}}(r_{200}, r_s)$, we assume average realistic uncertainties for current lensing surveys $\sigma_{r_{200}}/r_{200} = 0.1$ and $\sigma_{r_s}/r_s = 0.3$, with a correlation $\rho = 0.5$. As in e.g., [7,8], we work with the rescaled variables

$$\mathcal{Q}_2 = \frac{\mathcal{Q}}{1+\mathcal{Q}}, \quad \phi_2 = 1 - \exp\left[\frac{-\phi_\infty}{(M_{\text{P}}c_l^2 10^{-4})}\right], \tag{12}$$

which spawn the range $[0,1]$. In Figure 2 we have plotted the resulting $2\sigma$ (darker areas) and $3\sigma$ (lighter areas) allowed regions in the space $(\phi_2, \mathcal{Q}_2)$ for three relevant cases.
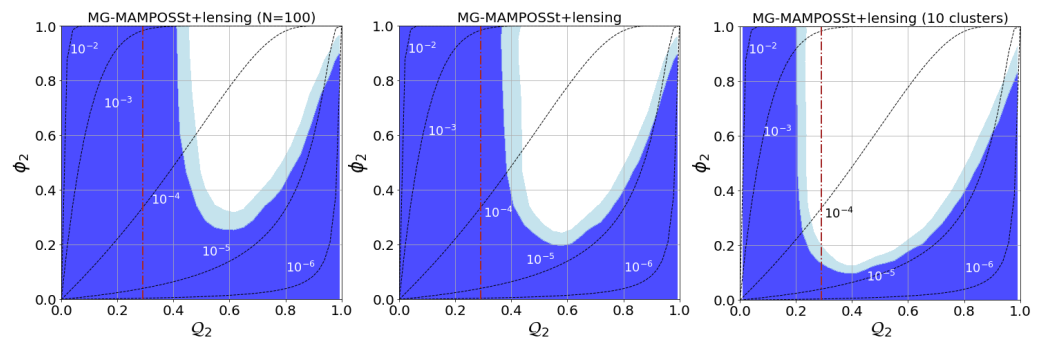


**Figure 2.** Results for the joint lensing and internal kinematics analysis of the synthetic haloes in our sample. The shaded areas show the allowed regions in the plane $(\mathcal{Q}_2, \phi_2)$ at $3\sigma$ (outer region) and $2\sigma$ (innermost region). (**Left panel**): 100 tracers in the MG-MAMPOSST fit. (**Central panel**): 600 tracers in the MG-MAMPOSST fit. (**Right panel**): combination of 10 clusters, 600 tracers considered in each halo. The black dashed curves are lines of constant $\phi/\mathcal{Q}$ while the vertical brown dash-dotted lines indicate value of the coupling $\mathcal{Q} = 1/\sqrt{6}$ corresponding to $f(\mathcal{R})$ gravity. From [22].

These results are very similar to that of [7,8] who performed joint X-rays and weak lensing analyses of galaxy clusters, but in the case of MG-MAMPOSST plus lensing, the excluded region is shifted towards larger values of $\mathcal{Q}_2$. This difference is related to the fact that hot X-ray-emitting gases in clusters and member galaxies are subject to distinct physical processes, despite the fact that they perceive the same gravitational potential. Note that the constraints show only a mild dependence on the number of tracers in the p.p.s., as the strength of the results relies on the additional (lensing) information on $r_s$ and $r_{200}$, needed to break the statistical degeneracy between the mass profile parameters and the MG parameters in internal kinematic analysis. When increasing the number of haloes in the fit (left panel in Figure 2, the bounds on the allowed region are noticeably tightened.

As a last step, we focus on the popular $f(\mathcal{R})$ gravity subclass of chameleon models, where $\mathcal{Q} = 1/\sqrt{6}$. In these framework, the fifth force is carried out by the derivative of the function with respect to the Ricci scalar, $f_\mathcal{R} = \partial f/\partial \mathcal{R}$, which acts as a scalar field generally known as scalaron. The present-day background value of the scalaron $f_{\mathcal{R}0}$ is connected to the chameleon field $\phi_\infty$ through (e.g., [8,17]):

$$\phi_\infty = -\sqrt{\frac{3}{2}}\ln(1 + f_{\mathcal{R}0})M_{\text{P}}c_l^2 \tag{13}$$

where $c_l$ is the speed of light. We perform the same kinematic and lensing analysis as for the general chameleon case described above, to constrain the value of the background scalaron field. It is worth pointing out that the constraints on $f(\mathcal{R})$ gravity derived with this approach are independent of the choice of the function $f$ (see [7,22]). The marginalized distributions of $\phi_\infty$ obtained in different cases are shown in Figure 13 of [22] for the combined analysis of 10 haloes. We further list the constraints for $f_{\mathcal{R}0}$ at 95% C.L. in the last two columns of Table 1 when varying the number of haloes considered in the fit. As in CS framework, the screening radius depends on the mass and the density of the sources (i.e., on $r_s$ and $r_{200}$), we have also generated p.p.s. from a less massive halo with a smaller concentration, characterized by $r_{200} = 1.41\,\mathrm{Mpc}$ and $r_s = 0.33\,\mathrm{Mpc}$. The marginalized 10-halo distribution is shown by the blue curve in Figure 13 of [22] What we found is that, as expected, smaller clusters exhibit a less efficient screening mechanism, allowing us to better constrain possible departures from GR.

As a final result of our forecast, we claim $|f_{\mathcal{R}0}| \lesssim 1.12 \times 10^{-5}$ and $|f_{\mathcal{R}0}| \lesssim 7.11 \times 10^{-6}$ at 95% C.L. from the joint lensing and internal kinematics analysis of 10 clusters and 20 clusters, respectively, when 600 tracers are considered in the MG-MAMPOSST fit and $\sigma_{r_{200}}/r_{200} = 0.1$, $\sigma_{r_s}/r_s = 0.3$ in the lensing distribution. For the less massive haloes, we obtain $|f_{\mathcal{R}0}| \leq 5.40 \times 10^{-6}$ and $|f_{\mathcal{R}0}| \leq 3.56 \times 10^{-6}$ for 10 and 20 clusters.

## 5. Discussion and Conclusions

We have introduced the main features of the license-free code MG-MAMPOSST, developed to constrain modified gravity models with the internal kinematic analysis of galaxy clusters, further equipped with simple lensing simulations for the two classes of scalar tensor theories currently implemented, chameleon screening and Vainsthein screening. The tests performed over mock haloes show that the combination of internal kinematic and lensing analyses provides promising results, even for a limited number of clusters. In particular, the relativistic coupling $Y_2$ in Vainsthein screening can be constrained with uncertainties of a few percent with a dozen clusters, assuming reliable high-quality kinematics and lensing information. The exercise has been pushed forward by using the currently available data of the massive galaxy cluster MACS 1206; in this case, we obtain $Y_2 = -0.12^{+0.66}_{-0.67}$ (see [37]), in agreement with GR prediction and comparable to other constraints at cluster scales for these models [9,26].

In a similar fashion, the allowed region in the parameter space of chameleon gravity $(\phi_2, \mathcal{Q}_2)$ can be strongly tightened with joint lensing and internal kinematic analyses of a few galaxy clusters, in a way which is complementary to cluster mass determinations using X-ray analyses of the hot intra-cluster gas (e.g., [7,8]). This indicates that the combination of kinematics of member galaxies, X-rays and lensing probes could provide very strong constraints on the behavior of gravity at cluster scales.

So far, we have investigated the constraining power of the MG-MAMPOSST method, assuming that all the systematics are under control. However, deviations from the dynamical relaxation assumption, crucial for the Jeans' analysis in clusters, as well as departures from spherical symmetry, can in principle affect the bounds on the model parameters, giving rise to spurious detection of modified gravity. Calibration and estimation of systematic effects is fundamental in view of the large amount of imaging and spectroscopic data that will be available in the near future. In [38], we showed that the analysis of cluster-size dark matter haloes in a $\Lambda$CDM universe indicates departures from GR in $\sim$70% of cases. Nevertheless, we also found that this percentage can be drastically decreased by looking at the distribution of member galaxies in the p.p.s and the line-of-sight velocity distribution $P(v_z)$. In particular, deviations from Gaussianity in $P(v_z)$, quantified by the so-called Anderson–Darling coefficient $A^2$ [39], are strongly related to the probability of finding suitable clusters for the application of our method. This is the case of MACS 1206, characterized by a small value of $A^2 \sim 0.6$, in agreement with a nearly Gaussian velocity distribution.

Given the current capabilities and limitations of our method, several improvements can be made, which will be available within the next versions of the MG-MAMPOSST code.

In particular, gravitationally bounded structures in some modified gravity theories may not be correctly described by an NFW profile (see, e.g., [40] and references therein). As such, we are planning to extend the parametrizations of the modified gravitational potentials to other mass models which may provide a better description of haloes in MG frameworks. Moreover, the efficiency of the screening mechanism depends on the shape of the matter distribution (e.g., [41]); thus, one should go beyond the assumption of spherical symmetry in computing the orbits with the Jeans' equation, in order to fully characterize the dynamics in these MG models. Finally, our forecast analysis has been performed on synthetic phase spaces generated in GR to explore the constraining power of MG-MAMPOSST. More realistic constraints can be obtained by computing orbits of member galaxies directly in a modified gravity scenario and comparing the results to real observational data. This can be conducted with the new version of the CLUSTERGEN code we are developing, which will be made publicly available in the future together with MG-MAMPOSST.

**Institutional Review Board Statement:** Not applicable.

**Informed Consent Statement:** Not applicable.

**Data Availability Statement:** The MG-MAMPOSST code is publicly available. A test p.p.s. data-set from a synthetic halo is shipped with the code. The data of MACS 1206 are partially provided by [30,42] by permission. Data will be shared on reasonable request to the corresponding author with the permission of CLASH-VLT collaboration: [36].

**Conflicts of Interest:** The author declare no conflicts of interest.

## Notes

1    https://github.com/Pizzuti92/MG-MAMPOSSt. (accessed on 25 January 2022), see [13] for the basic usage of the code.
2    In the literature the coupling constant is often indicated by $\beta$. However, as $\beta(r)$ also denotes the velocity anisotropy profile in kinematic analyses of galaxy clusters, we adopt $\mathcal{Q}$ for the coupling to avoid confusion.
3    The public version of MAMPOSST can be found at https://gitlab.com/gmamon/MAMPOSSt, accessed on 25 January 2022.
4    Note that $r_\nu$ is in general different from $r_s$ as the distribution of galaxies in clusters may not follow the distribution of the total matter (e.g., [28]).
5    In principle CLUSTERGEN can be used to produce mock clusters adopting different modified gravity setups and matter density distributions. In the exercise presented here we focus only on an NFW profile in GR as our fiducial model.

## References

1.    Saridakis, E.N.; Lazkoz, R.; Salzano, V.; Vargas Moniz, P.; Capozziello, S.; Beltrán Jiménez, J.; De Laurentis, M.; Olmo, G.J.; Akrami, Y.; Bahamonde, S.; et al. Modified Gravity and Cosmology: An Update by the CANTATA Network. *arXiv* **2021**, arXiv:2105.12582.
2.    Deffayet, C.; Gao, X.; Steer, D.A.; Zahariade, G. From k-essence to generalised Galileons. *arXiv* **2011**, arXiv:1103.3260.
3.    Zumalacárregui, M.; García-Bellido, J. Transforming gravity: From derivative couplings to matter to second-order scalar-tensor theories beyond the Horndeski Lagrangian. *arXiv* **2013**, arXiv:1308.4685.
4.    Amendola, L.; Bettoni, D.; Pinho, A.M.; Casas, S. Measuring gravity at cosmological scales. *Universe* **2020**, *6*, 20. [CrossRef]
5.    Koyama, K.; Sakstein, J. Astrophysical Probes of the Vainshtein Mechanism: Stars and Galaxies. *Phys. Rev. D* **2015**, *91*, 124066. [CrossRef]
6.    Cataneo, M.; Rapetti, D. Tests of gravity with galaxy clusters. *Int. J. Mod. Phys. D* **2018**, *27*, 1848006–1848936. [CrossRef]
7.    Terukina, A.; Lombriser, L.; Yamamoto, K.; Bacon, D.; Koyama, K.; Nichol, R.C. Testing chameleon gravity with the Coma cluster. *J. Cosmol. Astropart. Phys.* **2014**, *1404*, 013. [CrossRef]
8.    Wilcox, H.; Bacon, D.; Nichol, R.C.; Rooney, P.J.; Terukina, A.; Romer, A.K.; Koyama, K.; Zhao, G.; Hood, R.; Mann, R.G.; et al. The XMM Cluster Survey: Testing chameleon gravity using the profiles of clusters. *Mon. Not. R. Astron. Soc.* **2015**, *452*, 1171–1183. [CrossRef]

9.   Sakstein, J.; Wilcox, H.; Bacon, D.; Koyama, K.; Nichol, R.C. Testing Gravity Using Galaxy Clusters: New Constraints on Beyond Horndeski Theories. *J. Cosmol. Astropart. Phys.* **2016**, *1607*, 019. [CrossRef]

10.  Pizzuti, L.; Sartoris, B.; Borgani1, S.; Amendola, L.; Umetsu, K.; Biviano, A.; Girardi, M.; Rosati, P.; Balestra, I.; Caminha, G.B.; et al. CLASH-VLT: Testing the Nature of Gravity with Galaxy Cluster Mass Profiles. *J. Cosmol. Astropart. Phys.* **2016**, *1604*, 023. [CrossRef]

11.  Pizzuti1, L.; Sartoris, B.; Amendola, L.; Borgani1, S.; Biviano, A.; Umetsu, K.; Mercurio, A.; Rosati, P.; Balestra, I.; Caminha, G.B.; et al. CLASH-VLT: Constraints on $f(R)$ gravity models with galaxy clusters using lensing and kinematic analyses. *J. Cosmol. Astropart. Phys.* **2017**, *1707*, 023. [CrossRef]

12.  Mamon, G.A.; Biviano, A.; Boué, G. MAMPOSSt: Modelling Anisotropy and Mass Profiles of Observed Spherical Systems—I. Gaussian 3D velocities. *Mon. Not. R. Astron. Soc.* **2013**, *429*, 3079–3098. [CrossRef]

13.  Pizzuti, L.; Saltas, I.D.; Biviano, A.; Mamon, G.; Amendola, L. MG-MAMPOSSt, a code to test gravity at galaxy-cluster scales: A technical introduction. *arXiv* **2022**, arXiv:2201.07194.

14.  Buchdahl, H.A. Non-linear Lagrangians and cosmological theory. *Mon. Not. R. Astron. Soc.* **1970**, *150*, 1. [CrossRef]

15.  Khoury, J. Chameleon field theories. *Class. Quantum Gravity* **2013**, *30*, 214004. [CrossRef]

16.  Burrage, C.; Sakstein, J. Tests of chameleon gravity. *Living Rev. Relativ.* **2018**, *21*, 1–58. [CrossRef] [PubMed]

17.  Brax, P.; van de Bruck, C.; Davis, A.C.; Shaw, D.J. f(R) gravity and chameleon theories. *Phys. Rev. D* **2008**, *78*, 104021. [CrossRef]

18.  Navarro, J.F.; Frenk, C.S.; White, S.D.M. A Universal Density Profile from Hierarchical Clustering. *Astrophys. J.* **1997**, *490*, 493. [CrossRef]

19.  Peirani, S.; Dubois, Y.; Volonteri, M.; Devriendt, J.; Bundy, K.; Silk, J.; Pichon, C.; Kaviraj, S.; Gavazzi, R.; Habouzit, M. Density profile of dark matter haloes and galaxies in the HORIZON-AGN simulation: The impact of AGN feedback. *Mon. Not. R. Astron. Soc.* **2017**, *472*, 2153–2169. [CrossRef]

20.  Wilcox, H.; Nichol, R.C.; Zhao, G.B.; Bacon, D.; Koyama, K.; Romer, A.K. Simulation tests of galaxy cluster constraints on chameleon gravity. *Mon. Not. R. Astron. Soc.* **2016**, *462*, 715–725. [CrossRef]

21.  Dima, A.; Vernizzi, F. Vainshtein Screening in Scalar-Tensor Theories before and after GW170817: Constraints on Theories beyond Horndeski. *Phys. Rev.* **2018**, *D97*, 101302. [CrossRef]

22.  Pizzuti, L.; Saltas, I.D.; Amendola, L. mg-mamposst: A code to test modifications of gravity with internal kinematics and lensing analyses of galaxy clusters. *Mon. Not. R. Astron. Soc.* **2021**, *506*, 595–612. [CrossRef]

23.  Saltas, I.D.; Sawicki, I.; Lopes, I. White dwarfs and revelations. *J. Cosmol. Astropart. Phys.* **2018**, *1805*, 028. [CrossRef]

24.  Sakstein, J. Astrophysical tests of screened modified gravity. *Int. J. Mod. Phys.* **2018**, *D27*, 1848008. [CrossRef]

25.  Haridasu, B.S.; Karmakar, P.; De Petris, M.; Cardone, V.F.; Maoli, R. Testing generalized scalar-tensor theories of gravity with clusters of galaxies. *arXiv* **2021**, arXiv:2111.01101.

26.  Laudato, E.; Salzano, V.; Umetsu, K. Multi-component DHOST analysis in galaxy clusters. *arXiv* **2021**, arXiv:2110.11019.

27.  Mamon, G.A.; Łokas, E.L. Dark matter in elliptical galaxies—II. Estimating the mass within the virial radius. *Mon. Not. R. Astron. Soc.* **2005**, *363*, 705–722. [CrossRef]

28.  Mamon, G.A.; Cava, A.; Biviano, A.; Moretti, A.; Poggianti, B.; Bettoni, D. Structural and dynamical modeling of WINGS clusters. II. The orbital anisotropies of elliptical, spiral, and lenticular galaxies. *Astron. Astrophys.* **2019**, *631*, A131. [CrossRef]

29.  Tiret, O.; Combes, F.; Angus, G.W.; Famaey, B.; Zhao, H.S. Velocity dispersion around ellipticals in MOND. *Astron. Astrophys.* **2007**, *476*, L1–L4. [CrossRef]

30.  Umetsu, K.; Zitrin, A.; Gruen, D.; Merten, J.; Donahue, M.; Postman, M. CLASH: Joint Analysis of Strong-lensing, Weak-lensing Shear, and Magnification Data for 20 Galaxy Clusters. *Astrophys. J.* **2016**, *821*, 116. [CrossRef]

31.  Pizzuti, L.; Saltas, I.D.; Casas, S.; Amendola, L.; Biviano, A. Future constraints on the gravitational slip with the mass profiles of galaxy clusters. *Mon. Not. R. Astron. Soc.* **2019**, *486*, 596–607. [CrossRef]

32.  Kazantzidis, S.; Magorrian, J.; Moore, B. Generating Equilibrium Dark Matter Halos: Inadequacies of the Local Maxwellian Approximation. *Astrophys. J.* **2004**, *601*, 37–46. [CrossRef]

33.  Vasiliev, E. Agama reference documentation. *arXiv* **2019**, arXiv:1802.08255.

34.  Laureijs, R.; Amiaux, J.; Arduini, S.; Auguères, J.; Brinchmann, J.; Cole, R.; Cropper, M.; Dabin, C.; Duvet, L.; Ealet, A.; et al. Euclid Definition Study Report. *arXiv* **2011**, arXiv:1110.3193.

35.  Postman, M.; Coe, D.; Benítez, N.; Bradley, L.; Broadhurst, T.; Donahue, M.; Ford, H.; Graur, O.; Graves, G.; Jouvel, S.; et al. The Cluster Lensing and Supernova Survey with Hubble: An Overview. *Astrophys. J.* **2012**, *199*, 25. [CrossRef]

36.  Rosati, P.; Balestra, I.; Grillo, C.; Mercurio, A.; Nonino, M.; Biviano, A.; Girardi, M.; Vanzella, E.; Clash-VLT Team. CLASH-VLT: A VIMOS Large Programme to Map the Dark Matter Mass Distribution in Galaxy Clusters and Probe Distant Lensed Galaxies. *Messenger* **2014**, *158*, 48–53.

37.  Pizzuti, L.; Saltas, I.D.; Umetsu, K.; Sartoris, B. Probing Vainsthein-screening gravity with galaxy clusters using internal kinematics and strong and weak lensing. *arXiv* **2021**, arXiv:2112.12139.

38.  Pizzuti, L.; Sartoris, B.; Borgani, S.; Biviano, A. Calibration of systematics in constraining modified gravity models with galaxy cluster mass profiles. *J. Cosmol. Astropart. Phys.* **2020**, *04*, 024. [CrossRef]

39.  Anderson, T.W.; Darling, D.A. Asymptotic Theory of Certain. *Ann. Math. Statist.* **1952**, *6*, 193–212. [CrossRef]

40.  Corasaniti, P.S.; Giocoli, C.; Baldi, M. Dark matter halo sparsity of modified gravity scenarios. *Phys. Rev. D* **2020**, *102*, 043501. [CrossRef]

41. Burrage, C.; Dombrowski, J.; Saadeh, D. The shape dependence of Vainshtein screening in the cosmic matter bispectrum. *J. Cosmol. Astropart. Phys.* **2019**, *2019*, 023. [CrossRef]
42. Biviano, A.; Rosati, P.; Balestra, I.; Mercurio, A.; Girardi, M.; Nonino, M.; Grillo, C.; Scodeggio, M.; Lemze, D.; Kelson, D.; et al. CLASH-VLT: The mass, velocity-anisotropy, and pseudo-phase-space density profiles of the z = 0.44 galaxy cluster MACS J1206.2-0847. *Astron. Astrophys.* **2013**, *558*, A1. [CrossRef]